

# Self-Assembly of Single Diamond Surface Networks

Qingqing Sheng<sup>†</sup>, Hao Chen<sup>†</sup>, Wenting Mao, Congcong Cui, Shunai Che and Lu Han<sup>\*</sup>

**Abstract:** Biological scaffolds with hyperbolic surfaces, especially single gyroid and single diamond structures, have sparked immense interest for creating novel materials due to their extraordinary physical properties. However, the ability of nature to create these unbalanced surfaces has not been achieved in either lyotropic liquid crystals or block copolymer phases due to their thermodynamical instability in these systems. Here, we report the synthesis of a porous silica scaffold with a single diamond surface structure fabricated by self-assembly of the poly(ethylene oxide)-*b*-polystyrene-*b*-poly(L-lactide) and silica precursors in a mixed solvent of tetrahydrofuran and water. The single diamond structure with tetrahedral interconnected frameworks was revealed by the electron crystallographic reconstruction. We assume that the formation of single networks is induced by the structural transition through double diamond/single gyroid structures and related to the energetic change due to the fluctuations of the Gaussian curvature. This work may provide new insights into these biologically relevant surfaces and related self-assembly systems.

In nature, triply periodic hyperbolic surface nanostructures with negative Gaussian curvature, formed by natural evolutionary assembly, have been widely discovered.<sup>[1]</sup> Specifically, the single gyroid (SG,  $I_4I_32$ ,  $Q^{214}$ ) structure discovered in butterfly wing scales exhibits a complete photonic bandgap with polarization-dependent optical properties and negative refractions,<sup>[2]</sup> while the single diamond (SD,  $Fd\bar{3}m$ ,  $Q^{227}$ ) found in the exoskeletons of beetles and weevils is known as the “champion” photonic structure to date with the widest photonic bandgap.<sup>[3]</sup> The elegance of these unique structures has inspired many attempts to mimic this natural phenomenon.

These delicate structures have been achieved by physical methods such as three-dimensional (3D) printing, holographic lithography and direct laser writing or obtained by the replication of biological scaffolds as hard templates.<sup>[4]</sup> However, balanced triply periodic minimal surfaces (TPMSs) have been generally reported in chemical synthesis as thermodynamically stable phases, which are realized as the double network structures.<sup>[5]</sup> Three basic categories of TPMSs include double gyroid (DG,  $Ia\bar{3}d$ ,  $Q^{230}$ ), double diamond (DD,  $Pn\bar{3}m$ ,  $Q^{224}$ ) and the “plumber’s nightmare” double primitive (DP,  $Im\bar{3}m$ ,  $Q^{229}$ ).<sup>[6]</sup>

Despite the astonishing structural control in nature by the selective deposition of chitin into one of two non-intersecting water-channel networks embedded with the ordered smooth endoplasmic reticulum TPMS template,<sup>[7]</sup> the power of nature to create unbalanced single

networks has been only preliminarily realized in chemical synthesis and remains a significant challenge. Nevertheless, the construction of these single networks in solution from bottom-up self-assembly strategies is of fundamental importance not only for creating novel functional materials but also for providing a way to understand biological processes in nature.

Single-network structures, including SG and SD, have been obtained by the partial occupancy of the initially formed double-network template.<sup>[8]</sup> However, the “alternating” version of the double networks using ABC triblock terpolymers is considered an effective method.<sup>[9]</sup> The alternating gyroid  $G^A$  phases, the two networks of which are formed by chemically distinct A and C blocks and therefore reveal the same space group  $I_4I_32$  as SG, have been examined extensively. Notably, SG can be directly synthesised by the triblock terpolymer and silica precursor in solution.<sup>[10]</sup> Although the alternating diamond  $D^A$  structure has been shown to be a stable region in theoretical calculations of symmetric ABC triblock terpolymer systems,<sup>[11]</sup> there is no experimental report of SD formation in either the lyotropic liquid crystal phases or the block copolymeric systems. Only one example of SD is represented in thermotropic liquid crystals by the self-assembly of bolaamphiphiles with swallow-tailed lateral chains.<sup>[12]</sup>

Here, we report the direct fabrication of SD silica scaffolds by the multilayer core-shell micro-phase separation method. A triblock terpolymer poly(ethylene oxide)-*b*-polystyrene-*b*-poly(L-lactide) (PEO<sub>117</sub>-*b*-PS<sub>332</sub>-*b*-PLLA<sub>57</sub>) was used as the template, and tetraethyl orthosilicate (TEOS) was used as a silica source under acidic conditions in a mixture of tetrahydrofuran (THF) and aqueous HCl solution. The template molecule was synthesized by atom-transfer radical polymerization and ring-opening polymerization with a total molar mass of 44.0 kg/mol (polydispersity index of 1.88) and volume fractions of 11.0%, 80.9%, and 8.1% for the PEO, PS, and PLLA blocks, respectively (characterizations of the polymer are shown in Supporting Information, Figure S1 and S2, and Table S1). The Flory–Huggins interaction parameters were calculated as  $\chi_{\text{PLLA-PS}} \approx 128.4$ ,  $\chi_{\text{PLLA-PEO}} \approx 5.6$ , and  $\chi_{\text{PS-PEO}} \approx 80.5$  (Supporting Information, Table S3). The template molecule was dissolved in the common solvent THF due to the similarity of the solubility parameters of the three blocks (Supporting Information, Table S2) and THF ( $\delta = 18.6 \text{ [J cm}^{-3}\text{]}^{1/2}$ ). Microphase separation occurred upon the addition of an aqueous hydrochloric acid solution, as the hydrophobic blocks PLLA and PS are insoluble in water ( $\delta = 47.80 \text{ [J cm}^{-3}\text{]}^{1/2}$ ). The hydrophobic blocks PLLA and PS were in the THF-rich phase, and the hydrophilic block PEO was present in the H<sub>2</sub>O-rich phase to form hyperbolic surface networks. The silicate species would be hydrolysed and condensed to form the silica scaffold in the H<sub>2</sub>O-rich phase through the co-interaction of hydrogen bonding between PEO and silanol and the electrostatic interaction between  $\text{EO}_m\text{-}[(\text{EO})\cdot\text{H}_3\text{O}^+]_y$  and  $[\text{yCl}^-\text{Si}^+\text{OH}^{2+}]$ .<sup>[13]</sup> The template molecules were removed via calcination (Supporting Information, Figure S3). The template was stable and did not degrade within the synthesis time (Supporting Information, Figure S1).

Figure 1a shows the small angle X-ray scattering (SAXS) pattern of the calcined material. The ordering of the structure can be affected by the lattice/basis fluctuations and the overlapping of reflections with very small  $q$  value, only a few reflections can be indexed as indicated by black tick marks. The main structure was later determined by electron microscopy to be the shifted double diamond (SDD) scaffold with space

- [a] Q. Sheng,<sup>[†]</sup> W. Mao, Prof. Dr. S. Che  
School of Chemistry and Chemical Engineering, State Key Laboratory of Metal Matrix Composites, Shanghai Jiao Tong University  
800 Dongchuan Road, Shanghai, 200240 (P.R. China)
- [b] Q. Sheng,<sup>[†]</sup> C. Cui, Prof. Dr. S. Che, Prof. Dr. L. Han  
School of Chemical Science and Engineering, Tongji University, 1239  
Siping Road, Shanghai, China, 200092 (P. R. China)  
E-mail: [luhan@tongji.edu.cn](mailto:luhan@tongji.edu.cn)
- [c] Dr. H. Chen<sup>[†]</sup>  
Institut für Numerische und Angewandte Mathematik, Georg-August-Universität Göttingen, Lotzestr. 16-18, Göttingen 37083, Germany
- [†] These authors contributed equally to this work.

Supporting information for this article is given via a link at the end of the document.

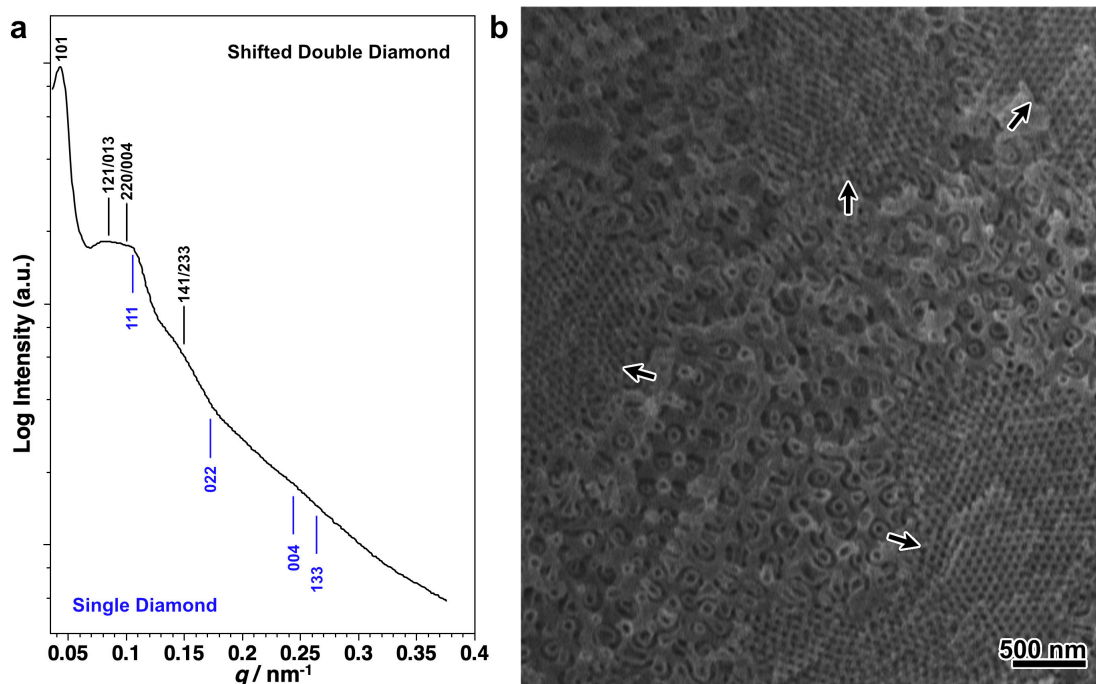


**Figure 1.** SAXS pattern and low-magnification SEM image of the product. a) SAXS pattern of the calcined material. b) SEM image of the calcined product, in which single network structures can be found as indicated by arrows. High-magnification SEM images of the corresponding structures are shown in Supporting Information Figure S5.

group tetragonal  $I4_1/amd$  (No. 141). The unit cell parameters are  $a_{\text{SDD}} = 185$  nm and  $c_{\text{SDD}} = 260$  nm  $\approx \sqrt{2}a_{\text{SDD}}$ . The SDD structure is similar to our previous report, which is formed by shifting cubic DD frameworks to achieve lower symmetry.<sup>[10a, 14]</sup> The unit cell parameter  $c_{\text{SDD}} = 260$  nm is twice of the unshifted original cubic DD with  $a_{\text{DD}} = 130$  nm. The scanning electron microscopy (SEM) image of the sample is shown in Figure 1b, revealing the overall information on the sample. The SDD structure is the main phase, which consists of domain structures with different crystal orientations (Supporting Information, Figure S4). However, small regions corresponding to the SD structure are often observed hundreds of nanometres to several micrometres in size, which are indicated by arrows (Supporting Information, Figures S5a and S5b). The unit-cell parameter of SD is determined to be  $a_{\text{SD}} \approx 100$  nm (vide post). The Bragg positions of the 111 and 400 reflections of the SD are indicated by blue tick marks in Figure 1a. Furthermore, a small amount of SG structure is also observed in the sample (Supporting Information, Figure S5c). The fluctuation of lattice size can be observed around the boundary between double and single networks, which leads to many stretched and distorted nodes as intermediate structures.

The high-magnification SEM images of the SD domain are shown in Figures 2a–2c. The framework structure contains only one set of networks, showing an interconnected scaffold structure, and each node is interconnected with four arms, revealing a 4-fold connected diamond network. Considering the geometry of the diamond structure, the arms of the framework run perpendicularly across the  $\{111\}_{\text{SD}}$  plane and are break easily. Therefore, the  $\{111\}_{\text{SD}}$  plane is easy to observe, and  $\{112\}_{\text{SD}}$  and  $\{100\}_{\text{SD}}$  are very rare.

The TEM images and the corresponding Fourier diffractograms (FDs) of the calcined sample taken from the  $[110]_{\text{SD}}$ ,  $[112]_{\text{SD}}$ ,  $[111]_{\text{SD}}$  and  $[100]_{\text{SD}}$  directions are shown in Figures 2d–2g, respectively. The observable reflection conditions are summarized as  $\{hkl: h+k, h+l, k+l \text{ even}\}$ ,  $\{0kl: k+l = 4n, k, l \text{ even}\}$ ,  $\{hhl: h+l \text{ even}\}$ , and  $\{00l: l = 4n\}$ , indicating  $Fd\bar{3}m$  symmetry (No. 227). The unit cell parameter calculated

from the SEM and TEM images is  $\sim 100$  nm. To reveal the 3D structure, an electrostatic potential map was obtained by electron crystallographic reconstruction. Both amplitudes and phases were extracted from the FDs of the TEM images along the  $[110]_{\text{SD}}$ ,  $[112]_{\text{SD}}$ ,  $[111]_{\text{SD}}$  and  $[100]_{\text{SD}}$  directions using the crystallographic image-processing software CRISP.<sup>[15]</sup> The proper area for taking FD was carefully chosen using the area selection tool in CRISP to exclude the very thin edge only contains half structure. The plane groups of  $c2mm$ ,  $p2mm$ ,  $p6mm$ , and  $p4mm$  were determined in the four directions (Supporting Information, Figure S6). The origin of the symmetry was chosen at the inversion centre (origin choice 2). The crystal structure factors were obtained by combining the four directions by scaling the amplitudes with the common reflections. The contrast transfer function was corrected by a Wiener filter to avoid zero division. Sixteen unique reflections were calculated to generate the 3D electrostatic potential map  $\varphi(x,y,z)$  by employing the software application VESTA<sup>[16]</sup> (Supporting Information, Table S4). A threshold for the equi-electrostatic potential surface was determined from the TEM images. Figure 2h presents the reconstructed 3D map of the unit cell, clearly showing the quadruple-linked networks grown along the diamond surface (Supporting Information, Figure S7). The hollow single-diamond frameworks can be clearly observed with a stick model superimposed on the hollow channels (Figure 2i). To verify the structure, the TEM images were simulated by the software MesoPoreImage<sup>[17]</sup> using a 3D continuum model of SD by nodal approximation.<sup>[18]</sup> The simulated TEM images from different zone axes are shown as insets in the TEM images in Figure 2. A good agreement of the experimental TEM images and the simulations suggests the faithfulness of the structural solution.

In our previous report, SG was formed directly by the cooperative self-assembly of an amphiphilic ABC triblock terpolymer poly(tert-butyl acrylate)-*b*-polystyrene-*b*-poly(ethylene oxide) (PEO-*b*-PS-*b*-PtBA) and silica precursor in a mixed solvent of tetrahydrofuran and water.<sup>[10a]</sup> The epitaxial intergrowth of DD and SG was observed with a

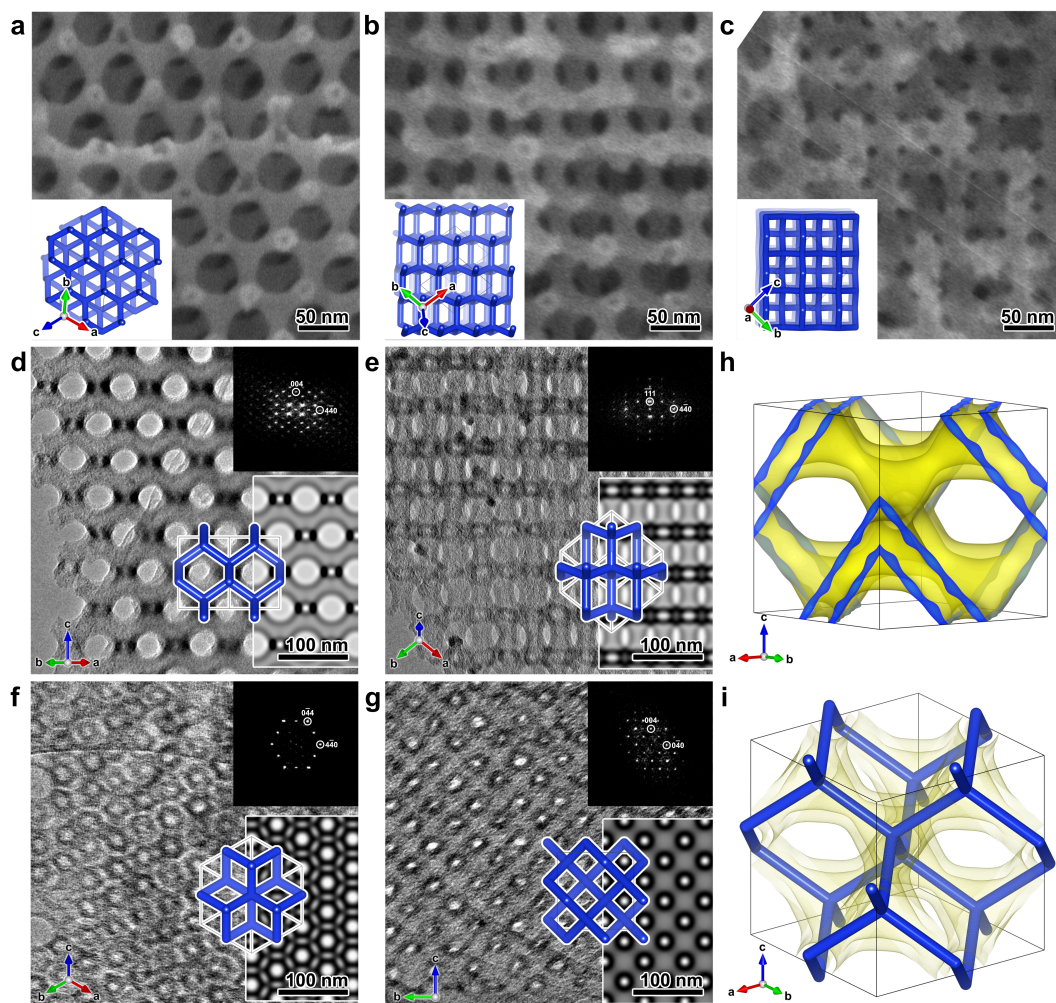


**Figure 2.** Structural characterizations of the SD structure. a-c) High-magnification SEM images taken of the  $\{111\}_{SD}$ ,  $\{112\}_{SD}$  and  $\{100\}_{SD}$  planes, respectively. The stick models are overlaid on the SEM images. d-g) TEM images and the corresponding FDs of the calcined sample were taken from the  $[110]_{SD}$ ,  $[112]_{SD}$ ,  $[111]_{SD}$  and  $[100]_{SD}$  directions, respectively. The insets show simulated TEM images using a 3-term nodal equation, and the stick models are overlaid on both the TEM and simulation to reveal the connectivity of the networks. h) Reconstructed 3D electrostatic potential map of a unit cell. i) 3D porous system with the stick model superimposed in the hollow channels, illustrating the four-fold connectivity of the porous structure.

unit cell relationship of  $SG/DD = \sqrt{2}/2$ . This relationship is far from the theoretical value of 1.57 in the Bonnett transformation,<sup>[6, 19]</sup> suggesting a great change in the Gaussian curvature. A further theoretical calculation by Sun *et al.* of the order-order phase transition path in an ABC triblock terpolymer system<sup>[10b]</sup> suggests the possibility of forming SG in a purely copolymeric system. Specifically, with the relatively weak interaction between the end blocks, an SG with a smaller unit cell size can be achieved, and the unit cell parameter relationship of  $SG/DD = \sqrt{2}/2$  is within the calculation range. The epitaxial relationship of DD and SG with a side-by-side relationship of  $(110)_{DD} // (100)_{SG}$  is also consistent with our experimental observations.<sup>[10a]</sup> The side-by-side relationship is also similar to the relationship between DD and DG.<sup>[20]</sup>

Inspired by these discussions, the epitaxial intergrowth and the structural relationship might be the key for the formation of the single network structure. The formation of the SD in this paper can be explained as follows.

i) The segregation of the three blocks follows the relationship of  $\chi_{PS-PLLA}N \gg \chi_{PEO-PS}N \gg \chi_{PEO-PLLA}N$ , which tends to form a microphase separation between the midblock (PS) and the end block (PEO/PLLA). This relationship is different from our previous paper<sup>[10a]</sup>, which employed PEO-*b*-PS-*b*-PtBA as a template with  $\chi_{AO}N \gg \chi_{SO}N \gg \chi_{AS}N$ .

The hydrophilic volume of PEO (11%) is in the range of 4–14.1 vol %),<sup>[21]</sup> which is favourable for the formation of bicontinuous structures. It is worthy to note that, the 3D hexagonally packed PLLA helices can be formed in PS-PLLA with volume fraction of  $f_{PLLA}^V = 0.35$ ,<sup>[22]</sup> which might affect the formation of SD in analogy to the chirality induced structural change in thermotropic liquid crystal networks of multi-chain compounds.<sup>[23]</sup> However, the as-synthesized product consisting both the triblock terpolymer and silica yields no circular dichroism (CD) signal by solid-state diffuse-reflectance CD (Supporting Information, Figure S8). In addition, while no helical structure corresponding to PLLA microdomain can be recognized in the TEM images of the as-synthesized product (Supporting Information, Figure S9). Therefore, no helical nanostructure of PLLA was formed herein and the formation of the SD is mainly determined by the microphase separation behavior related to the volume fraction of the different blocks. Besides, the SD structure cannot be synthesized using the conventional block copolymer PEO-*b*-PS or using PEO-*b*-PS-*b*-PLLA with a larger volume fraction of PLLA segments which may due to the undesirable disturbance of PLLA crystallization.

ii) The intergrown structure of DD and SD is obtained under the same synthesis conditions, suggesting that the free energy of each phase should be similar or that the barrier of the structural transition should be

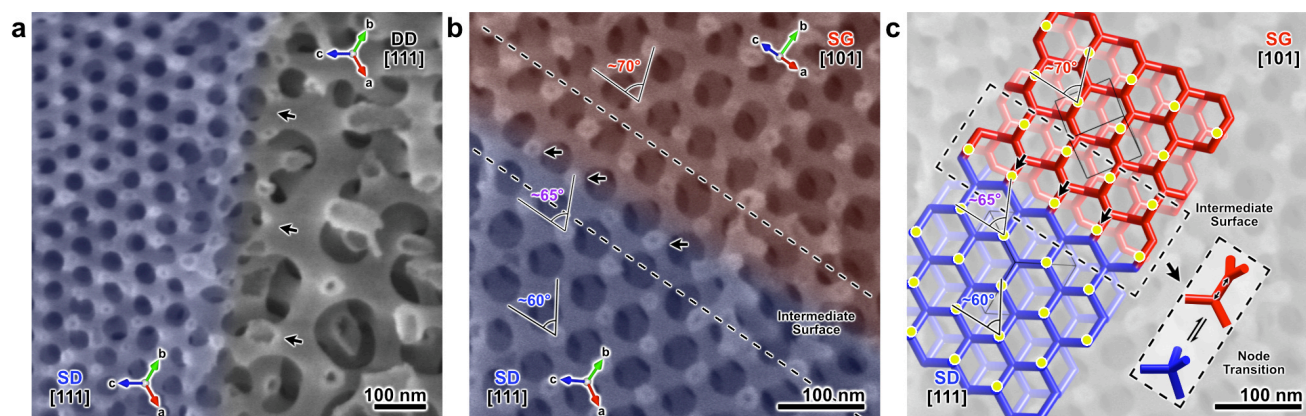


**Figure 3.** SEM images of the epitaxial relationship between different structures. a) SEM image of the epitaxial intergrowth of DD and SD. b) SEM images of the intergrown structure of SD and SG. c) Skeletal graph superimposed with the SEM image, representing the structural transition between the SD and SG structures.

small. This speculation can be supported by the theoretical calculation.<sup>[10b]</sup> Moreover, similar to our observation of SG structure, the intergrown structure may also be important for the formation of SD. The structural growth is restricted by the epitaxial relationship, and the structural relationship of DD to SD is  $a_{SD} : a_{DD} \approx \sqrt{3}$  and  $a_{DD} : a_{SD} \approx 1.3$ . The matching of the unit cell size for different phases further facilitates the epitaxial intergrowth process.<sup>[24]</sup>

iii) Neither SG nor SD is thermodynamically stable in the lyotropic liquid crystal phases or the block copolymer systems. In the thermotropic liquid crystalline system composed of solvent-free polyphilic molecules, SD was discovered as a stable thermodynamic minimum structure owing to the additional geometrical restriction provided by the molecular shape.<sup>[12]</sup> In ABC triblock terpolymer system, Sun *et al.* showed that SG is easily transformed to the HPL phase. Therefore, SG cannot be formed in a thermodynamic equilibrium process, and nucleation of the HPL phase must be prohibited to obtain SG.<sup>[10b]</sup> The same principle may also valid for the SD. To find proof for the structural formation, the products were freeze-dried and monitored as a function of reaction time (Supporting Information Figure S10). As the evaporation of solvents, the solid precipitate first appeared in the clarified solution after 40 h. The sample typically shows disordered hollow networks covered by the polymer template. The average distance between these hollow sections is close to 100 nm, which is similar to the structural scale of SD networks in the final product. After 48 h of aging, the DD phase appeared with much larger unit cell size surrounding the domains with small structural scale. The ordering of the small structure domain is also improved, which further turned into the SD structure. In the final product, the SD domains are often observed hundreds of nanometres to several micrometres in size and the main structure is DD. Based on the above observations, the formation of the structures can be speculated as follows. The disordered structure with small size was initially formed. Although it is difficult to determine the detailed geometry, the structure may close to the SD phase because of the similar lattice size. With the aging time, some of the small structure transformed to ordered SD following a curvature driven process while more regions turned into the DD phase due to its thermodynamic stability. This process is consistent with the theoretical calculation that the unstable SD can be easily transformed. In our case, the microphase separation is greatly changed due to the addition of inorganic precursors, and the reaction occurs under solvent evaporation. The structural formation is not only thermodynamically controlled but also a kinetic process. The unstable SD structure can be immobilised with silica condensation.

iv) Furthermore, according to the theoretical calculation by Qin *et*

*al.*,<sup>[11]</sup> the phase sequence of the structures is  $D \rightarrow S^A \rightarrow D^A \rightarrow G^A \rightarrow L$ , suggesting that the interfacial curvature of  $G^A$  is very close to that of  $D^A$ . By carefully tuning the synthesis conditions, the formation of SG may be the stepping stone for the successful synthesis of SD structures. Herein, we also occasionally discovered the intergrowth of the SG and SD. This intergrowth proved the structural similarity and will be discussed in detail.

We can imagine that the structural relationship of DD/SD, and SD/SG is the key to understanding the structural behaviour of the system. Figure 3a shows the SEM image of the intergrowth of DD and SD, revealing that the DD and SD share the same  $\langle 111 \rangle$  (corresponding to the  $\langle 110 \rangle$  direction of SDD) and  $\langle 001 \rangle$  directions. The formation of SDD is due to the loss of mutual support between the double frameworks with solvent evaporation<sup>[10a, 14]</sup>; thus, the original cubic symmetry cannot be maintained. However, unshifted cubic DD exists around the boundary, suggesting that the structural transition from DD to SD occurred at the very beginning of the reaction and that the original cubic symmetry was restricted by connectivity to the SD scaffold.

However, the transition of the SD and SG domains shows a similar unit cell parameter. As shown in Figure 3b (the low magnification SEM image is shown in Supporting Information, Figure S11), the two structures can be well connected with a side-by-side relationship with a  $\langle 111 \rangle_{DD} // \langle 101 \rangle_{SG}$  relationship by sharing the common  $\{121\}$  lattice plane. The unit cell parameter shows the relationship of  $a_{SD} : a_{SG} \approx 1.2$  (theoretical value of  $\sqrt{3}/\sqrt{2} = 1.225$ ). To clarify the structural interconversion, the skeletal graph representing the centres of the channel is constructed based on the SEM images. At the boundary, the intermediate structure can be clearly observed, in which the four-fold nodes of the D network are translated gradually into three-fold nodes along the  $\langle 001 \rangle_{SD}$  direction (Figure 3c). This structural change is compatible with an orthorhombic deformation of G<sup>[27a]</sup> and the principle of contracting edges in the deformation of labyrinthine nets proposed by Sadoc and Charvolin.<sup>[25]</sup>

The ubiquitous occurrence of diamond and gyroid structures is often explained by geometric homogeneities.<sup>[26]</sup> In particular, the corresponding D and G minimal surfaces are shown to minimize the fluctuation of the Gaussian curvature among all known TPMSs. We now analyse the SD-SG transition within this framework.

Following recent developments in differential geometry,<sup>[27]</sup> we view D and G TPMSs as consisting of necks among horizontal planes. In both cases, necks in each layer are arranged in a rhombic lattice. We normalize the edge length of the fundamental rhombus to 1. Then, the

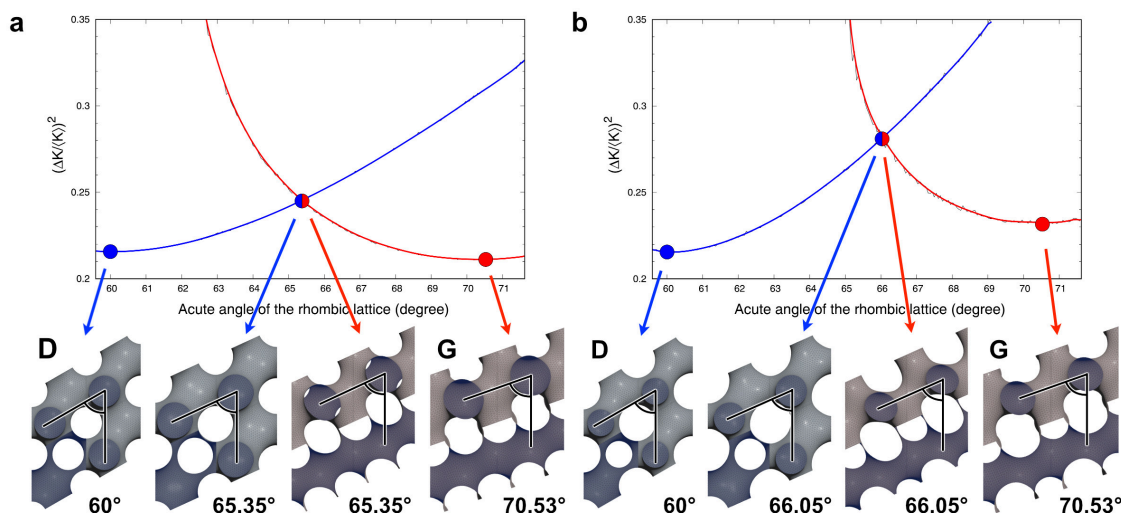


**Figure 4.** The fluctuation of the Gaussian curvature in the structural transition. a) The standard and deformed D and G minimal surfaces. b) The standard and deformed D and G CMC surfaces with 40% volume fraction.

vertical distance between adjacent planes is, conveniently,  $\sqrt{1/6}$  for both D and G. The lattices of D and G differ only in the acute angle  $\alpha$  of the fundamental rhombus, which is  $\pi/3 = 60^\circ$  for D and  $2\arctan(\sqrt{1/2}) \approx 70.529^\circ$  for G. With respect to the previous layer, each layer in the D surface is shifted by  $\sqrt{1/3}$  along the longer diagonal, while each layer in the G surface is shifted by  $1/2$  along and edges of the rhombus.

The normalized horizontal rhombic lattices and the identical vertical distances allow us to place D and G next to each other. However, there will be an abrupt change in the acute angle  $\alpha$ , which is physically unfavourable. The transition can be made smooth by first deforming the rhombic lattices of D and G to a compromising lattice with the same  $\alpha$ . Such a deformation could be an oDb deformation for D<sup>[28]</sup> and an orthorhombic deformation for G.<sup>[27a]</sup> To ensure energetic balance, the deformed D and G surfaces are expected to have the same fluctuation of Gaussian curvature.

To locate this compromising rhombus, deformations of the D and G minimal surfaces are generated in Surface Evolver<sup>[29]</sup> by minimizing the area subject to a constraint of 50% volume fraction. The acute angle  $\alpha$  is changed from 1.040 rad (59.59 degrees) to 1.250 rad (71.62 degrees) in steps of 0.001 rad. We then use the built-in squared Gaussian curvature energy to measure the normalized fluctuation  $(\Delta K/\langle K \rangle)^2$ , where K denotes the Gaussian curvature. The average Gaussian curvature  $\langle K \rangle$  depends only on the area (per fundamental unit). The result, as plotted in Figure 4a, indicates a transition at approximately  $\alpha = 1.142$  rad (65.43 degrees).

Changing the volume fraction to 40% yields constant mean curvature (CMC) surfaces, and the same measurement indicates a transition at approximately  $\alpha = 1.152$  rad (66.00 degrees); see the plot in Figure 4b. CMC surfaces are often considered a more realistic model for the neutral surfaces of bicontinuous block copolymer structures.<sup>[30]</sup> However, in our measurement, the 40% volume fraction is not meant to be precise, as the precise value is not available from the experiment. On the one hand, the 40% volume fraction ensures that the neutral surface is between the minimal surface and the silica scaffold. On the other hand, it is still possible to continuously deform the D and G CMC surfaces with a 40% volume fraction to the compromising lattice, which might not be the case with a smaller volume fraction. For instance, CMC gyroids might not exist with a volume fraction  $< 25\%$ .<sup>[31]</sup>

In summary, the SD silica scaffold was first synthesized by direct self-assembly using a triblock terpolymer as the template and silica

precursors in solvents. A detailed structural study by electron microscopy and curvature analysis showed that the structural transition and relationship between SD and the SG structure is the key factors for the formation of the SD phase and a small fluctuation of the Gaussian curvature may lead to the SD or SG structures. Therefore, the pure SD network can be expected by precisely controlling of the experimental conditions. Although it is still challenging to make practical material with optimized conditions at the current stage, our results show the possibility of creating these unbalanced biological structures in laboratories. The findings reported here may offer a platform to prepare novel structures and provide significant opportunities in the structural relationship of these biorelevant structures.

## Acknowledgements

This work was financially supported by the National Natural Science Foundation of China (Grant Nos. 21922304; L.H. 20931008, S.C.), Natural Science Foundation of Shanghai (Grant No. 18ZR1442400; L.H.), Fundamental Research Funds for the Central Universities (L.H.) and Deutsche Forschungsgemeinschaft (Grant No. 398759432; H.C.).

**Keywords:** single diamond surface structure • block copolymer • self-assembly • silica scaffold • electron microscopy

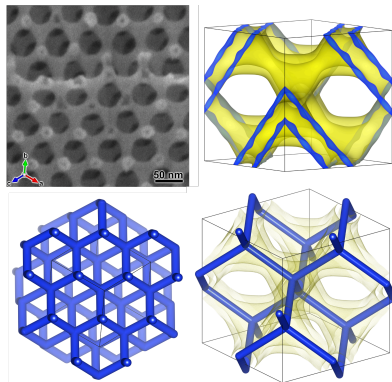
- [1] a) P. Vukusic, J. R. Sambles, *Nature* **2003**, *424*, 852-855; b) S. Tadeipalli, J. M. Slocik, M. K. Gupta, R. R. Naik, S. Singamaneni, *Chem. Rev.* **2017**, *117*, 12705-12763.
- [2] a) K. Michielsen, D. G. Stavenga, *J. R. Soc. Interface* **2008**, *5*, 85-94; b) J. A. Dolan, B. D. Wilts, S. Vignolini, J. J. Baumberg, U. Steiner, T. D. Wilkinson, *Adv. Opt. Mater.* **2015**, *3*, 12-32.
- [3] a) J. W. Galusha, L. R. Richey, J. S. Gardner, J. N. Cha, M. H. Bartl, *Phys. Rev. E* **2008**, *77*, 050904; b) M. Maldovan, E. L. Thomas, *Nat. Mater.* **2004**, *3*, 593-600.
- [4] a) M. Campbell, D. N. Sharp, M. T. Harrison, R. G. Denning, A. J. Turberfield, *Nature* **2000**, *404*, 53-56; b) S. Wong, M. Deubel, F. Pérez-Willard, S. John, G. A. Ozin, M. Wegener, G. von Freymann, *Adv. Mater.* **2006**, *18*, 265-269; c) J. W. Galusha, M. R. Jorgensen, M. H. Bartl, *Adv. Mater.* **2010**, *22*, 107-110.
- [5] L. Han, S. A. Che, *Adv. Mater.* **2018**, *30*, 1705708.
- [6] S. Andersson, S. T. Hyde, K. Larsson, S. Lidin, *Chem. Rev.* **1988**, *88*, 221-242.
- [7] a) V. Saranathan, C. O. Osuji, S. G. Mochrie, H. Noh, S. Narayanan, A. Sandy, E. R. Dufresne, R. O. Prum, *P. Natl. Acad. Sci. USA* **2010**, *107*, 11676-11681; b) B. Wilts, B. Apeleo Zubiri, M. Klatt, B. Butz,

- M. Fischer, S. Kelly, E. Spiecker, U. Steiner, G. Schröder-Turk, *Sci. Adv.* **2017**, *3*, e1603119.
- [8] a) H. J. Shin, R. Ryoo, Z. Liu, O. Terasaki, *J. Am. Chem. Soc.* **2001**, *123*, 1246-1247; b) Y. La, J. Song, M. G. Jeong, A. Cho, S. M. Jin, E. Lee, K. T. Kim, *Nat. Commun.* **2018**, *9*, 5327; c) M. Burton, A. Selvam, J. Lawrie-Ashton, A. Squires, N. Terrill, I. Nandhakumar, *ACS Appl. Mater. Interfaces* **2018**, *10*, 37087-37094.
- [9] a) S. Phan, G. H. Fredrickson, *Macromolecules* **1998**, *31*, 59-63; b) S. Vignolini, N. A. Yufa, P. S. Cunha, S. Guldin, I. Rushkin, M. Stefik, K. Hur, U. Wiesner, J. J. Baumberg, U. Steiner, *Adv. Mater.* **2012**, *24*, OP23-27.
- [10] a) X. Cao, D. Xu, Y. Yao, L. Han, O. Terasaki, S. Che, *Chem. Mater.* **2016**, *28*, 3691-3702; b) T. Sun, P. Tang, F. Qiu, Y. Yang, A.-C. Shi, *Macromol. Theor. Simul.* **2017**, *26*, 1700023.
- [11] J. Qin, F. S. Bates, D. C. Morse, *Macromolecules* **2010**, *43*, 5128-5136.
- [12] X. Zeng, S. Poppe, A. Lehmann, M. Prehm, C. Chen, F. Liu, H. Lu, G. Ungar, C. Tschierske, *Angew. Chem. Int. Ed.* **2019**, *58*, 7375-7379.
- [13] D. Zhao, Q. Huo, J. Feng, B. F. Chmelka, G. D. Stucky, *J. Am. Chem. Soc.* **1998**, *120*, 6024-6036.
- [14] L. Han, D. Xu, Y. Liu, T. Ohsuna, Y. Yao, C. Jiang, Y. Mai, Y. Cao, Y. Duan, S. Che, *Chem. Mater.* **2014**, *26*, 7020-7028.
- [15] M. Gemmi, P. Oleynikov, *Z. Krist. – Cryst. Mater.* **2013**, *228*, 51-58.
- [16] K. Momma, F. Izumi, *J. Appl. Cryst.* **2011**, *44*, 1272-1276.
- [17] T. Ohsuna, Y. Sakamoto, O. Terasaki, K. Kuroda, *Solid State Sci.* **2011**, *13*, 736-744.
- [18] P. J. F. Gandy, S. Bardhan, A. L. Mackay, J. Klinowski, *Chem. Phys. Lett.* **2001**, *336*, 187-195.
- [19] S. T. Hyde, S. Andersson, *Z. Krist. – Cryst. Mater.* **1985**, *170*, 225-239.
- [20] A. M. Seddon, J. Hallett, C. Beddoes, T. S. Plivelic, A. M. Squires, *Langmuir* **2014**, *30*, 5705-5710.
- [21] M. Stefik, S. Mahajan, H. Sai, T. H. Epps, F. S. Bates, S. M. Gruner, F. J. Disalvo, U. Wiesner, *Chem. Mater.* **2009**, *21*, 5466-5473.
- [22] a) R.-M. Ho, Y.-W. Chiang, C.-C. Tsai, C.-C. Lin, B.-T. Ko, B.-H. Huang, *J. Am. Chem. Soc.* **2004**, *126*, 2704-2705; b) R. M. Ho, C. K. Chen, Y. W. Chiang, *Macromol. Rapid Commun.* **2009**, *30*, 1439-1456;
- [23] C. Dressel, T. Reppe, S. Poppe, M. Prehm, H. Lu, X. Zeng, G. Ungar, C. Tschierske, *Adv. Funct. Mater.* **2020**, *30*, 2004353.
- [24] a) M. W. Matsen, *J. Chem. Phys.* **1998**, *108*, 785-796; b) J. Suzuki, K. Nakane, A. Takano, Y. Matsushita, *Polymer* **2004**, *45*, 8989-8997; c) N. Ji, P. Tang, F. Qiu, A.-C. Shi, *Macromolecules* **2015**, *48*, 8681-8693.
- [25] J.-F. Sadoc, J. Charvolin, *Acta Crystallogr.* **1989**, *A45*, 10-20.
- [26] G. E. Schröder-Turk, A. Fogden, S. T. Hyde, *Eur. Phys. J. B* **2007**, *54*, 509-524.
- [27] a) H. Chen, *Exp. Math.* **2019**, *28*, 404 - 419; b) H. Chen, M. Traizet, **2019**, *arXiv: 1908.06276*.
- [28] A. Fogden, S. T. Hyde, *Acta Crystallogr.* **1992**, *A48*, 575-591.
- [29] K. A. Brakke, *Exp. Math.* **1992**, *1*, 141-165.
- [30] M. W. Matsen, F. S. Bates, *J. Chem. Phys.* **1997**, *106*, 2436-2448.
- [31] K. Große-Brauckmann, *Exp. Math.* **1997**, *6*, 33-50.

Entry for the Table of Contents (Please choose one layout)

## COMMUNICATION

Silica scaffold with single diamond surface networks has been synthesized via self-assembly of the triblock terpolymer and inorganic source. The structural transition and the fluctuations of the Gaussian curvature are the key for the formation of the single diamond structure.



Q. Sheng, H. Chen, W. Mao, C. Cui, S. Che, L. Han\*

Page No. - Page No.

**Self-Assembly of Single Diamond Surface Networks**